

Exploiting LSPIV to assess debris flow velocities in the field

Joshua I. Theule^{1,3}, Stefano Crema², Lorenzo Marchi², Marco Cavalli², Francesco Comiti¹

¹Faculty of Science and Technology, Free University of Bozen-Bolzano, Bozen-Bolzano, 39100, Italy

²Research Institute for Geo-hydrological Protection, National Research Council of Italy, Padova, 35127, Italy

³TerrAlp Consulting, 100 chemin du grand pré, 38410 St Martin d'Uriage, France

Correspondence to: Joshua I. Theule (joshua.theule@terralpconsulting.com)

Abstract. The assessment of flow velocity has a central role in quantitative analysis of debris flows, both for the characterization of the phenomenology of these processes, and for the assessment of related hazards. Large scale particle image velocimetry (LSPIV) can contribute to the assessment of surface velocity of debris flows, provided that the specific features of these processes (e.g. fast stage variations and particles up to boulder size on the flow surface) are taken into account. Three debris flow events, each of them consisting of several surges featuring different sediment concentration, flow stage and velocity, have been analyzed at the inlet of a sediment trap in a stream of the eastern Italian Alps (Gadria Creek). Free softwares have been employed for preliminary treatment (ortho-rectification and format conversion) of video-recorded images as well as for LSPIV application. Results show that LSPIV velocities are consistent with manual measurements on the ortho-rectified imagery and with front velocity measured from the hydrographs in a channel reach approximately 70 m upstream of the sediment trap. Horizontal turbulence, computed as the standard deviation of the flow directions at a given cross-section for a given surge, proved to be correlated with surface velocity and with visually estimated sediment concentration. The study demonstrates the effectiveness of LSPIV in the assessment of surface velocity of debris flows, and permit to identify the most crucial aspects for improving the accuracy of debris flows velocity measurements.

1 Introduction

Debris flows are a rapid flow of saturated non-plastic debris in a steep channel (Hungr et al., 2001). They consist of poorly sorted sediments mixed with water and organic debris with sediment concentrations higher than 50% by volume or 70% by mass (Costa, 1984; Phillips and Davies, 1991) and can travel over long distances at relatively high velocities (generally between 2 to 20 m s⁻¹) (Iverson, 1997; Rickenmann, 1999). Debris flows are relatively infrequent and complex events which make it difficult to characterize their dynamic flow heights, velocities, discharge, and flow resistance of the material, among other aspects.

Debris-flow velocities and discharge are typically backcalculated from surveyed channel bends with superelevated flow heights using the forced vortex equation (eg. Hungr et al., 1984; Chen, 1987; Prochaska et al., 2008; Scheidl et al., 2014). The measured parameters (flow heights, velocity, and slope) from post-event surveys for this equation can also be used to estimate flow resistance coefficients to understand the viscosity and sediment concentrations of the debris flows (eg.

Rickenmann, 1999). However, sediment concentrations are known to significantly increase and decrease during the propagation of the flow (eg. Pierson and Scott, 1985; Rickenmann et al., 2003) and the velocity profile of the surges can also vary thus limiting the reliability of post-event field methods.

Debris-flow monitoring projects are growing thanks to the increasing feasibility and capability of observing several parameters of this complex process (eg. Marchi et al., 2002; Coe et al., 2008; Arattano et al., 2012; Navratil et al., 2013; Comiti et al., 2014). Typical monitoring stations consist of geophones, ultrasonic sensors (or radar), and video cameras which satisfy the basic measurements of velocity, height, discharge, and visual validation. Some catchments present also multiple stations distributed throughout the debris-flow channel and some located in headwater channels (Berti et al., 2000; Marchi et al., 2002; Hürlimann et al., 2003; McCoy et al., 2010; Arattano et al., 2012; Navratil et al., 2013; Comiti et al., 2014).

Video acquisitions originally started as a validation of the instrumented recordings and visual interpretation, but as cameras, power, and storage capacities improve, further analysis can be made. Manual tracking of particles with field measurements can measure velocities accurately when compared to stage sensors (eg. Arattano and Grattoni, 2000; Marchi et al., 2002). The video imagery of debris flow can also be used to interpret the turbulence, sediment mixture, sediment concentration, presence of rigid plugs and laminar flows (eg. Marchi et al., 2002). Horizontal velocity distributions from video imagery have shown variations of flow resistance between events and within the same surge (Genevois et al., 2001). Rheological parameters are known to significantly vary within the same surge, but they are very difficult to quantify in the field.

Large scale particle image velocimetry (LSPIV) is another video imagery technique often used in rivers to measure two dimensional velocities from high resolution images at high frame rates (eg. Fujita et al., 1998; Hauet et al., 2008; Le Coz et al., 2010; Muste et al., 2014). Cross-correlations are made between time-step imagery within a given search window. This is typically applied in steady flows by tracking bubbles, ice, debris, and artificial seeding. Discharge rates can then be estimated because of the stable cross-sections during the flow. LSPIV and series of elevation models were also compared during bedload transport flume experiments to quantify discharge and deposition, as well as Froude and Shield's numbers.

These types of analysis are difficult for debris flows because the different surges can vary in height and significantly modify the channel bed. The LSPIV method was tested on a pulsing flash flood in a stable reach from a GoPro recording that was available on Youtube (Le Boursicaud et al., 2016). There was a 3-5% velocity error for 15-30 cm water level bias which was the largest source of error in the analysis. Recently, a long-term discharge monitoring project of a mountain stream with LSPIV applications used an automated detection of the water level heights (Stumpf et al., 2016). This method still poses a problem for the highly irregular debris-flow surfaces, however considering the low percent error, approximate heights should be feasible for surface velocity. Laser profile scanners were also used in LSPIV applications for measuring debris-flow velocities with direct comparisons of flow heights providing accurate discharge measurements and analysis of the flow dynamics (Jacquemart et al., 2017).

To our knowledge, the application of LSPIV on debris flows from video images has not been deeply investigated whereas it could provide direct measurement to quantify rheological behavior of debris flows. Our objective is to test the LSPIV

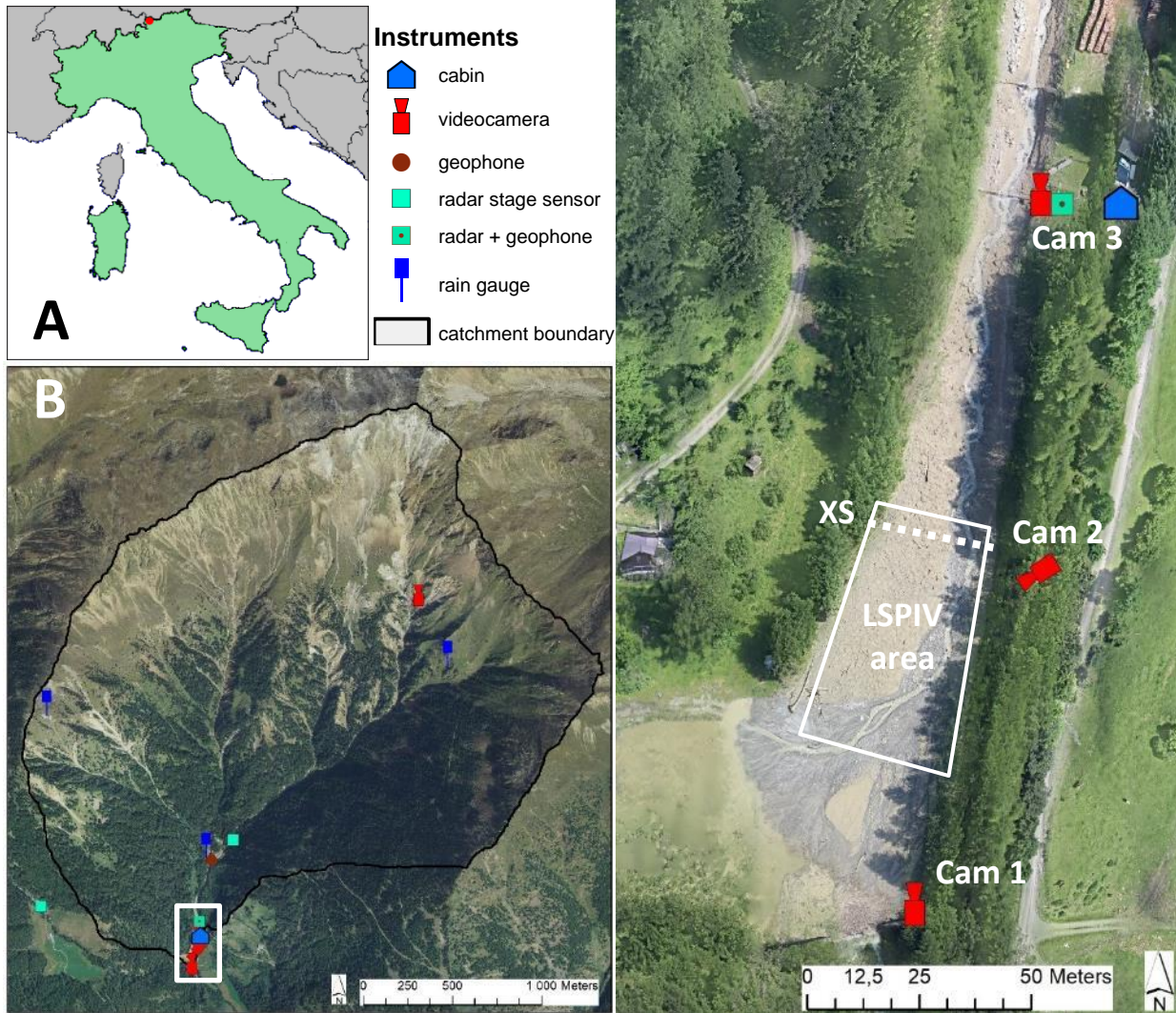
method on debris flows using available cameras in a monitored catchment in the Italian Alps (Gadria catchment) (Fig. 1). The aims of this work are to explore: 1) the spatial and temporal variation within one study reach of debris-flow surges occurred in the period 2013-2015, 2) a detailed analysis of an individual surge dynamic, 3) the quantification of a “horizontal turbulence index” (influenced by rheological parameters) from the directional variation of vectors, and 4) the limitations/perspectives of the LSPIV for further development.

2 Setting

The Gadria catchment is situated in Vinschgau-Venosta Valley (South Tyrol) in the Eastern Italian Alps (Fig. 1A), and features a drainage area of 6.3 km² (between 1394 and 2945 m a.s.l.), with an average slope of 79.1 %. The source area consists of highly deformed and fractured metamorphic rock, thick glacio-fluvial deposits and steep topography which makes the catchment prone to rockfall, landslides, avalanches and debris flows. The topographic settings of the catchment ensure an effective connectivity of sediment between the source areas (D’Agostino and Bertoldi, 2014) and the downstream channel reaches (Cavalli et al., 2013). Debris flows occur in the summer and are usually triggered by spatially-limited convective storms. The mean volume of the debris flows observed between 1979 and 2013 is 14,000 m³ (median 8000 m³) (Aigner et al., 2015). The sediment yield of the Gadria catchment between 2005 and 2011, a period normal as to frequency and magnitude of debris flows, was computed through DEM differencing (Cavalli et al., 2017) and amounted to about 5200 m³km⁻²yr⁻¹. Instrumented monitoring of the Gadria catchment began in 2011, for detailed information of the study site and monitoring setup, refer to Comiti et al. (2014).

Two cameras are alongside a sediment trap (retention basin) near the alluvial fan apex, one looking upstream (Cam1) and the other looking down at a more perpendicular angle to the flow (Cam2). The third camera (Cam3) is in the next reach upstream from the sediment trap at a closer proximity to the flow (Fig. 2). These three cameras are connected to a cabin equipped with power supply and a server (8 Tb storage capacity) collecting all the monitoring data. The fourth camera is in an upstream ravine and it is triggered by a rain gauge when there is at least one minute of rainfall. For this study, we focused on the application of LSPIV using only one of the four MOBOTIX M12 video cameras, Cam 2.

We attempted to utilize the other cameras for LSPIV application, but Cam 1 and Cam 3 were too close with an upstream view to measure the large scale of the debris flow. Within the area of high incidence angle of the images, the number of reference points is restricted, there is little spatial coverage, and there was too much pooling of water in front of Cam 1 located at the dam. Cam 2 was the best option because it was located higher on top of the levee (10 - 52% incidence angle), 12 - 46 m from the LSPIV area, and had an orientation more perpendicular to the flow path. Cam 4 was problematic due to the unchanneled nature of the recorded events, in combination with the relative long distance between the camera and the moving sediment.



102 **3 Methods**

103 The LSPIV methods that we used are based on Le Boursicaud et al. (2016). The previous study tested the LSPIV method on
104 a pulsating flashflood in the French Alps recorded from a GoPro. The videos were treated for photo stitching and format
105 conversion using freeware and the LSPIV calculation on the freeware Fudaa-LSPIV (Le Coz et al., 2014)
106 (<https://forge.irstea.fr/projects/fudaa-lspiv/files>).

107 **3.1 Video treatment**

108 The M12 Mobotix security camera that we used is an IP camera (resolution 1689x1345) with a fish eye lens, at night
109 spotlights are activated during rainfall. This camera has limiting features such as an automatic adjustment for shutter speed
110 with illumination, and therefore the frame per second cannot be fixed. This initially was a problem since our aim was to have
111 a constant 10 frame per seconds (fps). During recording of the flow events, the frequency reduced to 2 - 3 fps because of the
112 low lighting of the storms. We needed a standard frame rate for LSPIV calculations, therefore we subsampled the images to
113 the minimum frame rate of each flow event (Table 1).

114 Also, since the camera had a fisheye lens, significant distortion correction was required. A checkerboard pattern image from
115 the camera was used in a free software Hugin (<http://hugin.sourceforge.net>) which has a tool for distortion correction. This
116 was then applied to all the video imagery and converted to an ASCII grey scale format using batch processing in the XNview
117 freeware (www.xnview.com). This used to be necessary for the Fudaa software, however it now can handle jpeg and tiff
118 colored formats.

119 **3.2 Reference points using Structure from Motion Photogrammetry**

120 High-resolution colored point clouds from Structure from Motion (SfM) surveys were found to be very useful for matching
121 reference points with the video images (Fig. 2A). In active debris-flow channels, permanent points are difficult to keep
122 within the active area, and with oblique angled cameras, there needs to be as many reference points as possible. The
123 sediment trap and channel were surveyed before and after flow events by walking up and down the banks with a camera
124 mounted on a 5-m pole with georeferenced targets (measured by total station) distributed throughout the channel and trap.
125 The SfM photogrammetry using AgiSoft® Photoscan (eg. Westoby et al. 2012; Javernick et al., 2014; Piermattei et al. 2015)
126 was used to generate high resolution colored point clouds (1300-2900 pts/m³) with 2 cm alignment error (using an iterative
127 closest point algorithm on permanent features) making it a reliable spatial and visual reference. For the LSPIV purposes, the
128 point clouds were rotated to make an approximate horizontal flow plane (5-degree rotation) to reduce any added spatial error.
129 These flow planes are easily visible in the colored point clouds with distinct mudlines.

130

131

132 **Table 1: LSPIV parameters used for the 2013, 2014, 2015 events.**

	2013	2014	2015
resolution	5cm/pixel		
alignment error near the flow plane	3-10 cm	4-7 cm	8-13 cm
# reference points	13	13	14
interrogation area	26 pixel (1.3 m)		
search area (pixels)	75-100 down; 5 up; 35-50 left; 30-50 right		
time step	0.333 s	0.5 s	0.5 s
grid	0.4-1.2 m		
area	28-35 m long and 7-32 m wide		

133 **3.3 Fudaa LSPIV**

134 For orthorectifying the video images, targets and natural features were used as reference points for matching between the
135 SfM point cloud (both pre-event and post-event) and video imagery (Fig. 2A, 2B). Corners of rocks next to the flow line
136 were typically used on each side of the channel, and sometimes exposed stable rocks within the channel. Alignment errors of
137 the reference points (Table 1) in the orthorectification process of Fudaa-LSPIV increase going down and across the channel
138 according to the camera’s oblique angle. The flow plane elevation was also measured by averaging matched features
139 touching the flow line in the post-event point cloud, this is the best estimate for the rough variable surface of the flow height.
140 The unsteady flows also required separating the fronts and tails to redefine the flow plane elevation which is known to be the
141 largest source of error for LSPIV (Le Boursicaud et al., 2016).

142 The interrogation area (IA) is the boundary for calculating a correlation coefficient which needs to be representative of the
143 flow velocity (Fig. 2C). It should find the travel distance of general features in the flow between each time step, not
144 individual particles, which is unrealistic in irregular flows with sediment rolling and continuously being submerged. We used
145 a 26 x 26 pixel (1.3 m x 1.3 m) interrogation area for calculating the correlation coefficient and a search area of 75-100 pixel
146 (3.75 - 5 m) downstream, 60 - 100 pixel (3 - 5 m) wide, and a small 5 pixel segment upstream to capture flow towards the
147 banks.

148 To have a good spatial distribution of the flow with a manageable dataset, we selected a grid with an approximate spacing of
149 0.7 m (varies with flow width) (Fig. 2C). Within the Fudaa software, we filtered any velocities with a correlation coefficient
150 less than 0.5-0.6 for a robust dataset (Fig. 2D). The velocity vectors were transferred into ArcGIS and overlaid on the
151 corresponding orthorectified image for manual cleaning. Noisy data can occur outside of the flow area because of rain, wind,
152 changing light reflection on wetted surfaces. The manual treatment of the vectors was also necessary for outlining and
153 separating the different surges and parts of the surge (front and tail) traveling through the study reach.

154 The spatial distribution of velocity vectors covering the reach provided an opportunity to examine their variation (direction
155 and velocity fluctuation) to characterize the turbulence of the various debris-flow surges (Costa 1984). Since our LSPIV
156 method is in the two dimensions, we define it as the horizontal turbulence index according to directional variation (T_d) and
157 velocity variation (T_v). We measure the turbulence (T_d and T_v) by taking the standard deviation of vector orientations (T_d) and
158 velocities (T_v) in 3 adjacent cross-sections for three time steps. The given segment of cross-sections can be used to examine

159 the changing characteristics of the surges rather than the spatial distribution. Therefore, small T_v and T_d should characterize
160 laminar flow conditions and higher values should be associated to more turbulent flows.
161 The LSPIV results were taken from cross-section XS (Fig. 1C) to have accurate comparisons of debris flow surges. This is
162 the most stable cross-section before the widening in the sediment trap. It is also the closest and most perpendicular view
163 from the camera resulting in the most accurate LSPIV calculations. The LSPIV study reach experienced important
164 deposition and remobilization during the debris flow surges, therefore we did not attempt to measure the discharge rates.

165

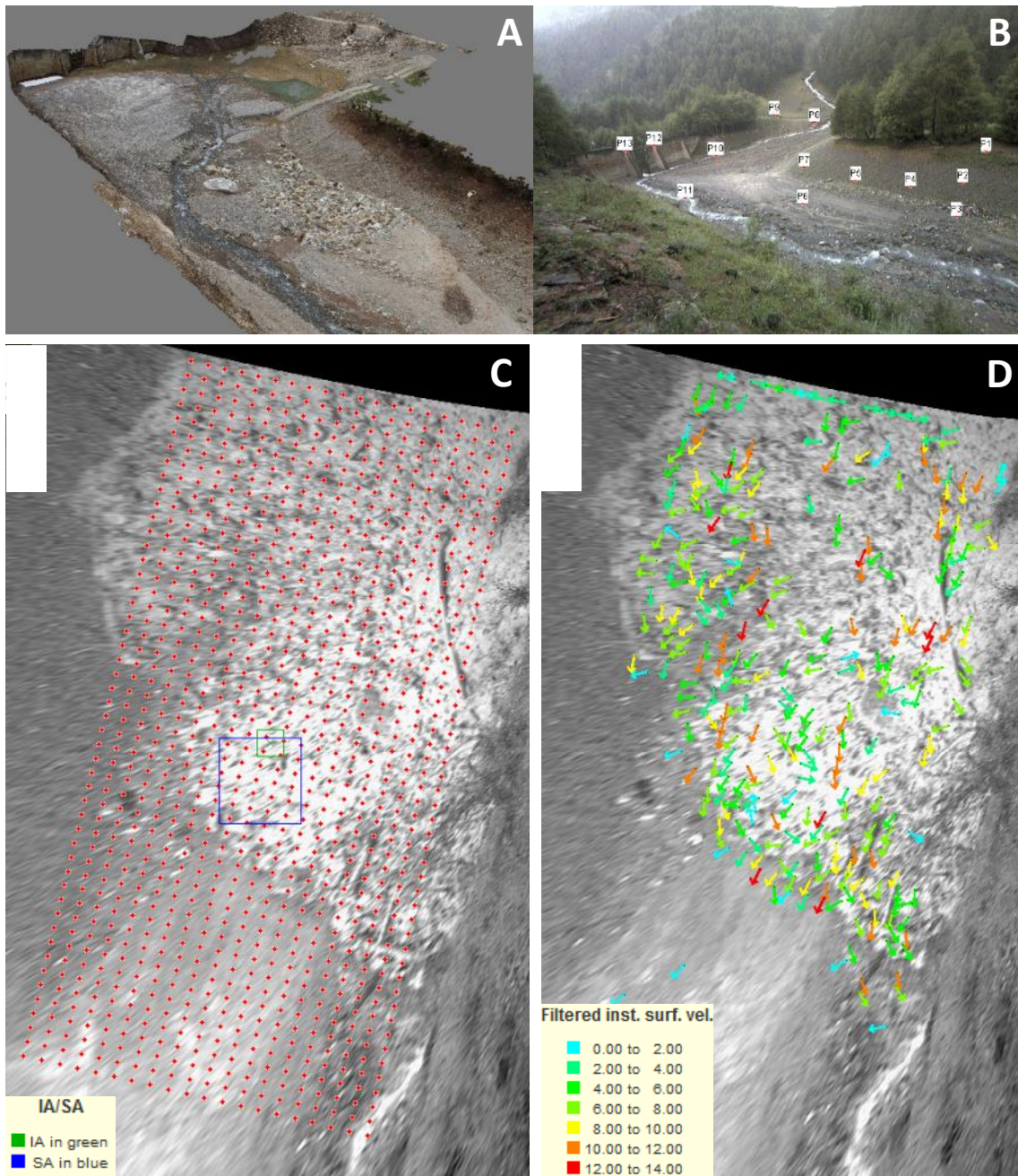


Figure 2: Example of (A) a SfM point cloud used as a post-event reference, (B) the undistorted camera image with the reference points, (C) the orthorectified image during the 2013 debris-flow front with the sampling grid, interrogation area (IA) and the search area (SA), and (D) the instantaneous surface velocity vectors.

171 **4 Analysed events**

172 In the 2011-2015 time span there have been four important events (Table 2; Fig. 3). The 2011 event was complex, with the
173 first and most important surge consisting of a hyperconcentrated flow and, only Cam 1 and Cam 3 were operational at the
174 time (Fig. 3). Therefore, LSPIV was not performed; measurements of flow velocity were performed manually (ratio of the
175 time interval between the passage of the front and the distance between the two radar sensors) and by means of cross-
176 correlation between the stage recordings (Comiti et al., 2014). There were no significant events in 2012.

177 The 2013 event featured one important surge, very typical debris-flow formation with a boulder front and the slurry-like tail.
178 The singular surge provided a convenient detailed analysis of the front, intermediate stage (transition from front to tail), and
179 the tail (described later).

180 The 2014 event had a small preliminary surge (pre-surge) and four debris flow surges passing through the study reach. It
181 should be noted that there was a discontinuous surge that stopped just upstream of the LSPIV measurements before the first
182 measured surge passed through the reach. The first two measured surges were large enough to distinguish the front (S1 and
183 S2) and tail (S1 tail S2 tail) and the latter two were too small and were kept undivided (S3 and S4). There seemed to be a
184 higher water content with longer sustained fronts (compared to 2013). The S4 was unusually fast which behaved more of a
185 wave passing through the filled-up sediment trap of highly saturated deposit.

186 The 2015 event was especially interesting because of the surges variable rheology. High-intensity rainfall covered the entire
187 catchment triggering many different source areas. The first surge (S1) had little sediment but carried a lot of large woody
188 debris. S2 was a slower muddier flow, however cobbles and boulders were also transported. S3 was a larger and even slower
189 muddy flow, carrying boulders, cobbles, and large woody debris. S4 is the slowest surge and a more visco-plastic flow still
190 carrying cobbles. S5 is similar to S4 but carried fewer cobbles. In between these surges the low-flow material stops, the
191 visco-plastic material waited for the next surge to push it forward. A low steady muddy flow continued for another 30 min
192 with smaller surges. However, the sediment trap became filled creating a saturated pool of sediment making surges difficult
193 to pass through.

194

195

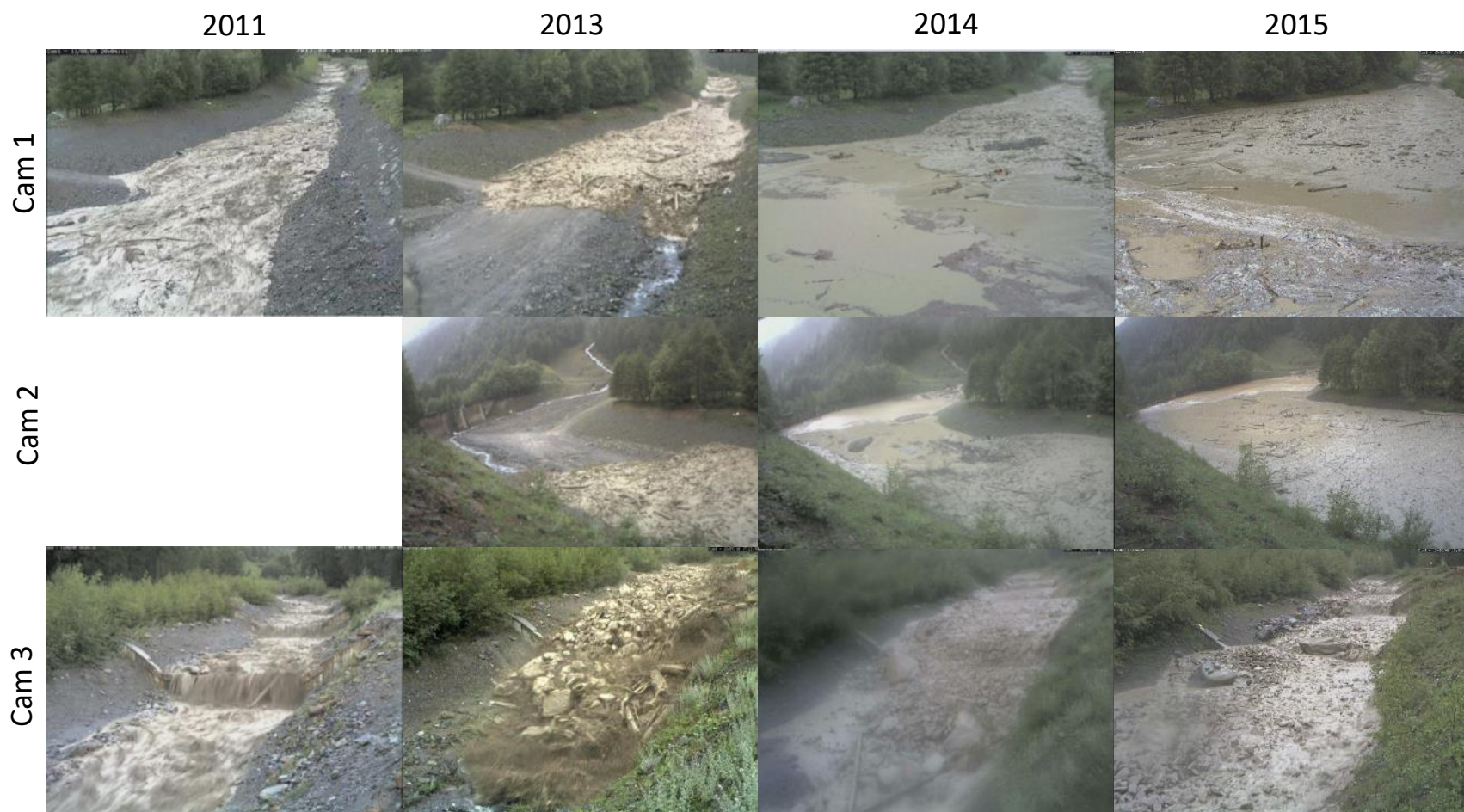


Figure 3: Views of the three cameras during the 2011, 2013, 2014 and 2015 debris flows. Cam 2 was selected for the LSPIV application due to the best positioning.

Table 2: Results of averaged LSPIV measurements, visual feature measurements on orthorectified images, and radar sensors (70 – 150 m upstream from the LSPIV section) for identifiable surges in 2011, 2013, 2014, 2015 (no events occurred in 2012).

Event	Surge	Time	LSPIV				Visual		Radar Sensors (70 m and 150 m upstream from LSPIV)	
			velocity (m s ⁻¹)	width (m)	T_d (degrees)	T_v (m s ⁻¹)	sediment concentration	velocity (m s ⁻¹)	velocity (m s ⁻¹)	avg height (m)
2011	HF surge	18:00 – 18:30	--	--	--	--	low	--	2.6	0.6
2013	S1 Front	17:23:10 – 17:23:26	4.4	19	24.5	2.7	high	4.4	5.7	1.9
	S1 Inter.	17:23:35 – 17:23:42	3.1	18	15.2	1.3	medium	2.4	--	1.6
	S1 Tail	17:23:43 – 17:24:05	1.9	17	24.6	1.3	medium	2.6	--	1.0
2014	Pre-surge	17:13:45 – 17:15:13	3.2	7	33.8	2.2	low	2.7	--	0.4
	S1*	17:22:01 – 17:22:17	4.6	23	36.0	2.8	medium	5.6	5.3	1
	S1 tail*	17:22:20 – 17:22:49	4.2	13	32.6	3.1	medium	4.4	4.8	0.5
	S2	17:25:43 – 17:26:04	3.1	22	32.3	2.8	high	3.3	4.1	0.9
	S2 tail	17:26:10 – 17:27:00	2.9	15	34.1	2.6	high	2.8	3.6	0.7
	S3	17:29:24 – 17:29:40	3.9	14	32.3	3.3	high	4.4	4.8	0.9
	S4 (wave)	17:30:13 – 17:30:21	6.2	8	31.3	4.2	low	6.9	3.5	0.7
2015	S1	17:16:52 – 17:17:15	5.6	14	33.2	3.0	low	4.9	--	0.8
	S2	17:20:05 – 17:21:02	2.5	17	30.7	2.8	high	3.0	3.5	0.8
	S3	17:23:30 – 17:24:01	2.2	22	29.2	2.5	high	1.5	3.5	1.25
	S4	17:24:25 – 17:25:12	0.6	20	21.5	1.1	very high	0.7	--	0.6
	S5	17:26:54 – 17:27:39	0.8	16	9.4	0.6	very high	1.0	--	0.8

* the first actual debris flow surge stopped between the LSPIV and the radar, it remobilized with S1.

205 **5 Results**

206 **5.1 Surface flow velocities**

207 LSPIV results of the three analysed debris flows were extracted from the upstream cross-section of the LSPIV reach (XS in
208 Fig. 1C). This makes surge comparisons more accurate because it is located in a more stable and confined location, rather
209 than the open sediment trap that fills up during the events. Mean surge velocities ranged from 0.6 to 6.2 m/s, velocity
210 variation turbulence (T_v) from 0.6 to 4.2 m/s, and directional variation turbulence (T_d) from 9.4 to 36.0 degrees (Table 2; Fig.
211 4). The instantaneous velocities for the 2013 event have smaller variations compared to the other events. The minimum
212 recording frequency was 3 fps for 2013 rather than 2 fps for 2014 and 2015 because of the available light during the storms.
213 The highest velocity (2014 S4) had a significantly higher T_v which is expected for a wave passing through a slurry.
214 The LSPIV velocities seem fairly accurate considering the low camera frequency (2-3 fps), camera angle, 5 cm/pixel
215 resolution and the unsteadiness of the flows. Their average velocities at a given cross-section were compared with manual
216 measurements of identifiable features on the same orthorectified images (feature picking) to validate the LSPIV cross-
217 correlation matching (Table 2; Fig. 5). The LSPIV has a slight under estimation with a mean difference of -0.1 m/s and a
218 standard deviation of 0.54 m/s. The LSPIV estimates are however more robust because of the large sample sizes and the
219 feature picking does not always represent the flow velocity accurately.
220 The LSPIV velocities are also compared with the velocities measured by the radar sensors 70 - 150 m upstream (located in
221 Fig. 1). Given the downstream decrease in velocity, the agreement is satisfactory, with a mean difference of -0.9 m/s and a
222 standard deviation of 0.25 m/s (Table 2; Fig. 5). Not all of the surges could be traced from the radar sensors to the LSPIV
223 reach, rather they will stop and be pushed by the next surge. This is especially the case with the visco-plastic surges in 2015.

224

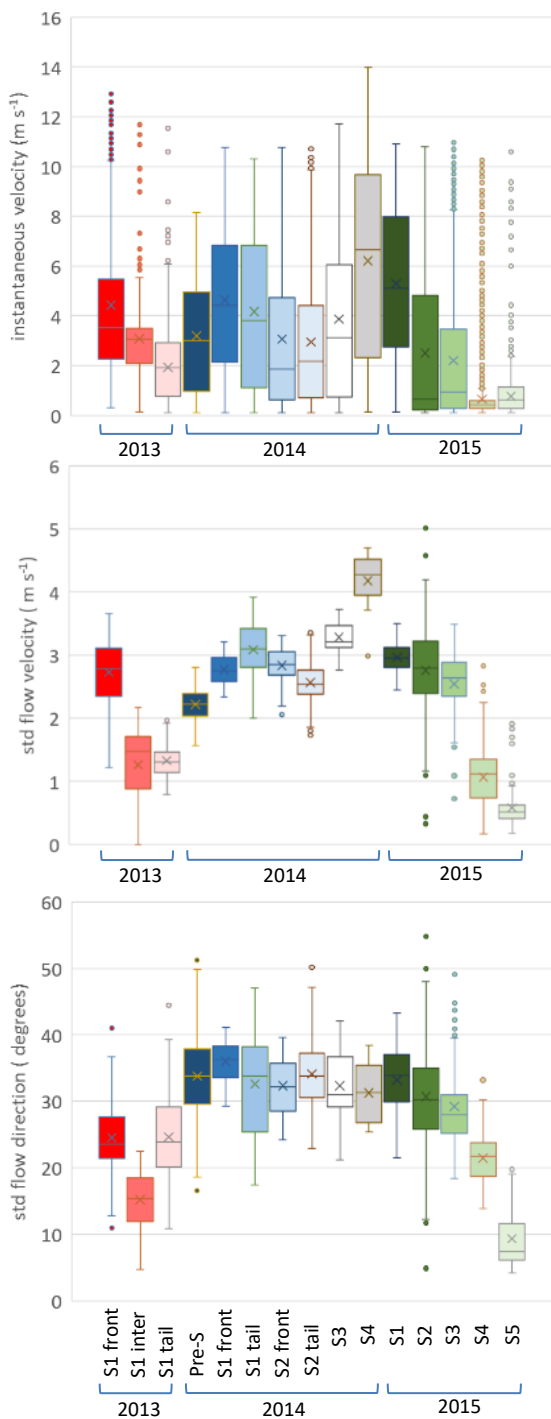


Figure 4: LSPIV velocity (top), velocity variation (T_v) (middle), and directional variation (T_d) (bottom) comparisons for 2013, 2014, 2015 surges located at the same cross-section.



231

233

235

236

250 These features correspond with the flow dynamics seen in Figure 7 with the boulder front depositing on the higher convex
251 features with the water surge passing around in the lower confined channel.

252 The longitudinal profile of the average velocities combined with the video imagery and multi-date topography (Fig. 8)
253 distinctly show the boulder front depositing after the sudden decrease in local slope (down to a negative slope) and channel
254 widening. The front average velocity remains constant even after the deposition of boulders. The intermediate part of the
255 surge shows the correspondence of the decreased velocity and the deposition. The boulder deposit narrows the channel and
256 therefore increases the velocity for the tail of the flow. The tail has an unusual increase of velocity at the downstream end
257 despite the local widening of the channel with decreasing velocity. Either there was a released plugging upstream or there
258 was an important decrease of sediment concentration (upstream deposition).

259 Several studies observe peak velocities of debris flows located behind the boulder front (Pierson, 1986; Arattano and Marchi,
260 2000; Suwa, 1993). The high concentration of the interlocking boulders creates a high frictional resistance and low mobility
261 (Pierson, 1986; Suwa, 1993). Debris flow channels typically have several reaches with important narrowing and widening
262 and naturally the velocity longitudinal profile must adjust to each channel reach. When the front is confined, boulders
263 interlock, velocities are higher behind the front as previous studies showed. In our case, we observe the boulders unlocking
264 which creates more mobility where the peak velocity is in the very front of the flow. The boulders laterally deposit as a levee
265 because of the decrease in transport capacity.

266

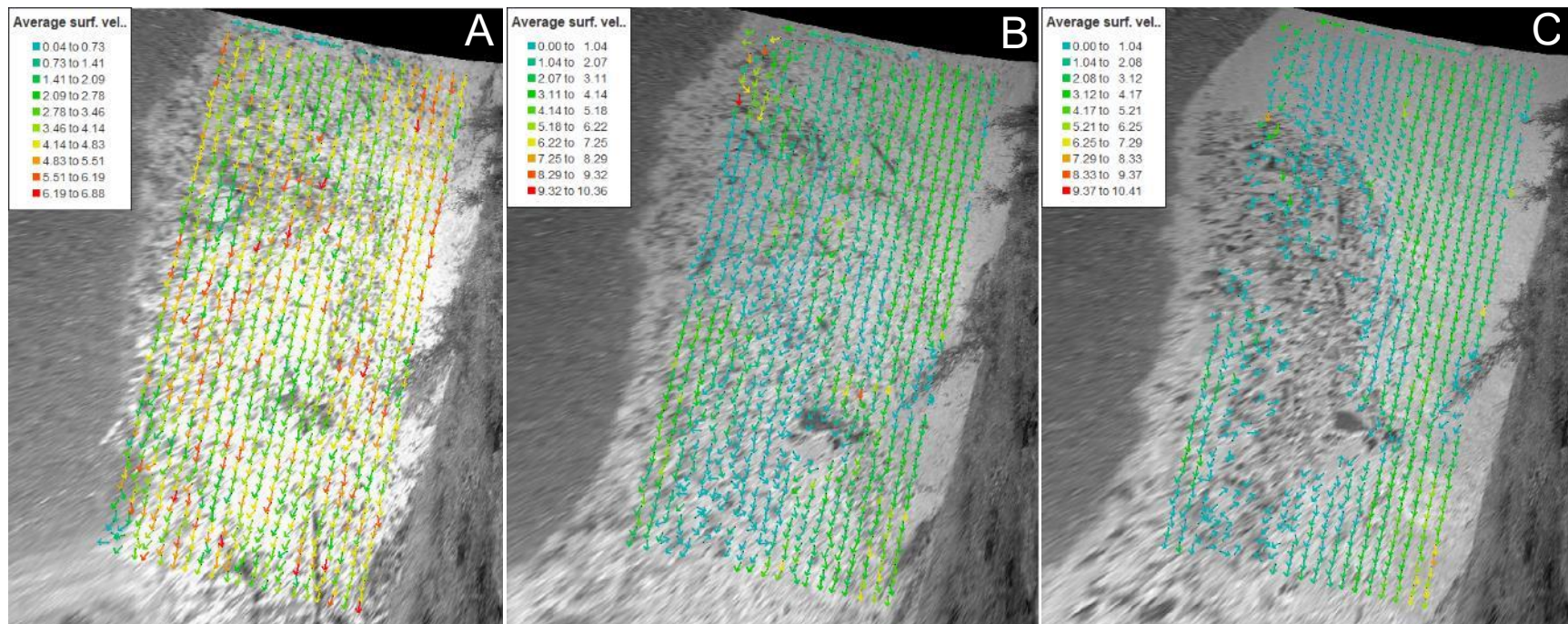


Figure 6: Average LSPIV velocities (m s^{-1}) for the 2013 debris-flow front (A) intermediate (B) and tail (C).

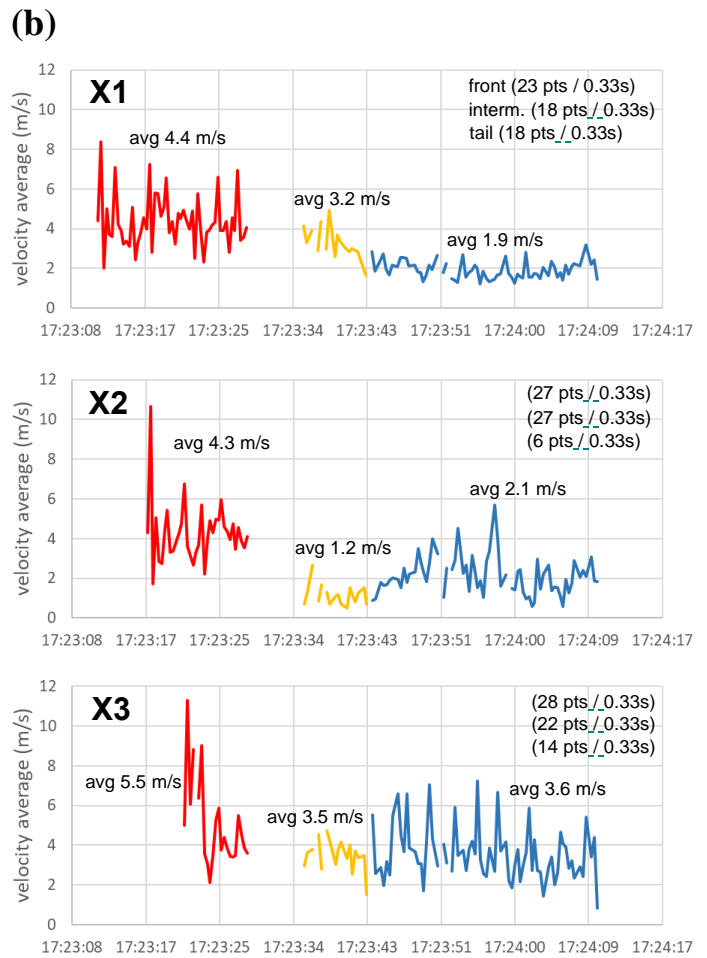
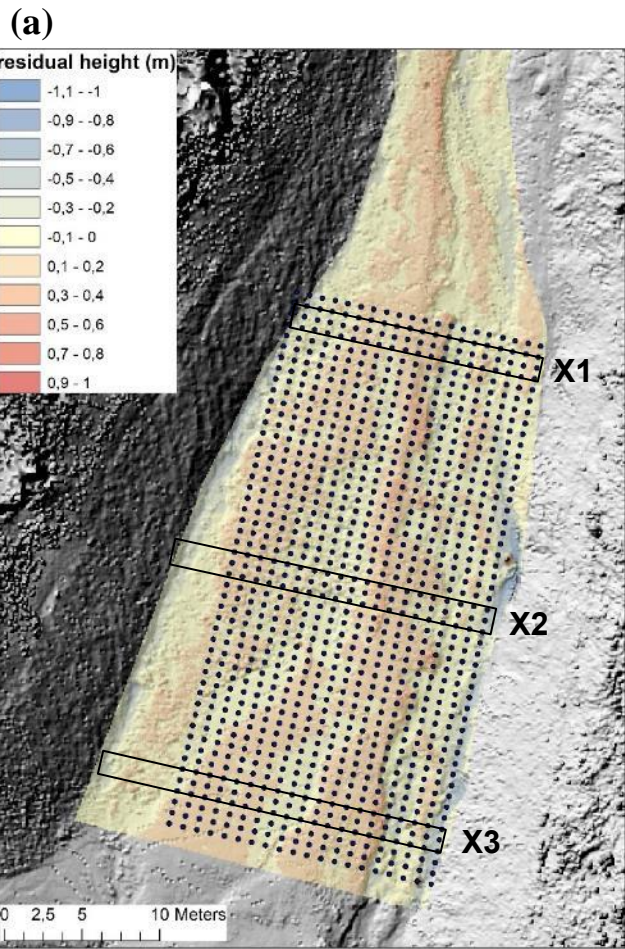


Figure 7: (a) Preliminary residual elevation of the channel bed at a 5-m scale, the grid of LSPIV calculations is shown with cross-section X1-3 outlined; (b) 2013 debris-flow LSPIV velocity time series (3 fps) at three cross-sections (X1, X2, and X3) with red (front), yellow (intermediate), and blue (tail). The velocity variation mostly represents the turbulence; however, some noise can come from low point density. The time interruption between the front and intermediate was initially made in the LSPIV analysis to clearly distinguish the two.

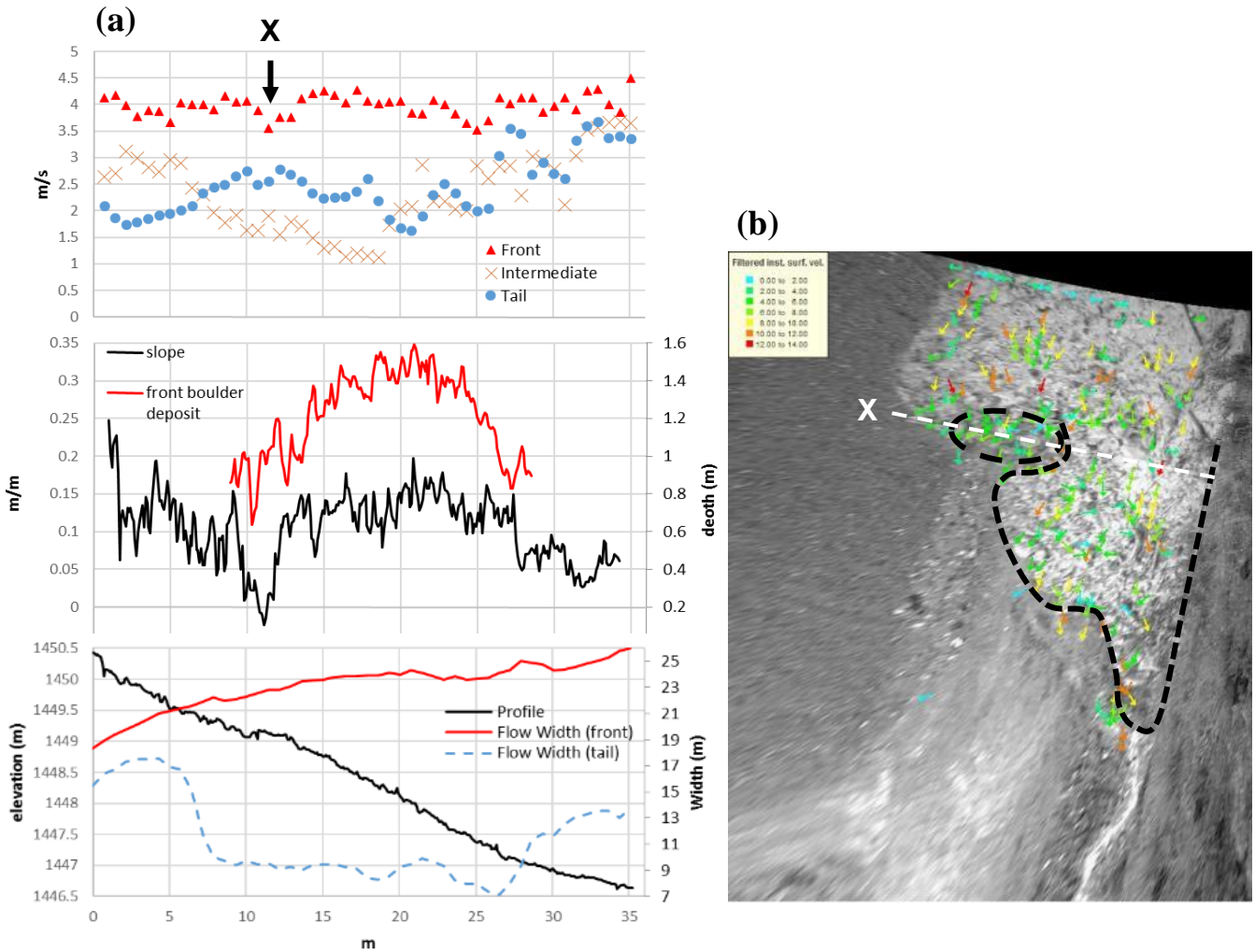


Figure 8: (a) The 2013 debris flow LSPIV average velocity of the front (red), intermediate (yellow), and tail (blue) traveling downstream (along the long profile of the grid in Figure 7). Local slope and the boulder front deposit (from multi-date SfM) are also plotted along the distance (center) as well as pre-event elevation and flow width of both the front and tail (bottom). At cross-section X, the boulder front is seen to deposit while the watery surge passes around it (b) which gives constant peak velocity in the front of the surge (despite the front deposition).

5.3 Horizontal turbulence index

Sediment concentration, viscosity, and yield strength are rheological parameters that can influence the turbulence and are commonly associated with flow resistance coefficients (eg. Rickenmann and Recking, 2011). For all the surges in 2013-2015, we found that turbulence has a strong relation with the surge velocity (Fig. 9), whereas flow heights and flow widths had much lower correlation with surge velocities. We compared both directional turbulence (T_d) and velocity turbulence (T_v) index measurements (see section 3.3) to the empirical flow resistance equation for debris flows from Koch et al. (1998), described in Rickenmann (1999):

$$C = \frac{V}{H^{0.3}S^{0.5}}, \quad (1)$$

where velocity (V) is the average LSPIV velocity for each surge, slope (S) being constant, flow height (H) measured upstream from the radar sensors (thereby introducing an additional source of error), and the flow resistance coefficient (C). The T_v clearly has a stronger correlation than the T_d when compared with V and C (Fig. 9). Based on the data analyzed, the power-law equation that links T_v to the flow velocity V through the coefficient C is:

$$V = 3.91T_v^{1.06}H^{0.3}S^{0.5}, \quad (2)$$

however, more surges need to be measured to better define the function. The influence of spatial and temporal sampling resolutions also needs to be better understood for further application.

Sediment concentrations from visual estimates (Table 2) were used to classify these comparisons which shows a better correspondence with T_v than T_d when comparing with C for the debris flow fronts. Sediment concentrations for the tails or waves did not correspond well, probably because of influences of fluid pressures from the front and the pooling of slurry in the sediment trap. Nonetheless, visual estimates of sediment concentrations are quite difficult, especially in highly turbulent conditions.

For some of the surges, boulders and logs can be seen rotating, resulting in misrepresentative flow directions and velocity fluctuations. Our interrogation area (1.3 m) for LSPIV calculations was aimed to characterize the general flow characteristics where these misrepresentations are either too detailed or have little influence on the high sampling of the LSPIV method. Higher image resolution and camera speed might give further insight on boulder dynamics and log jamming.

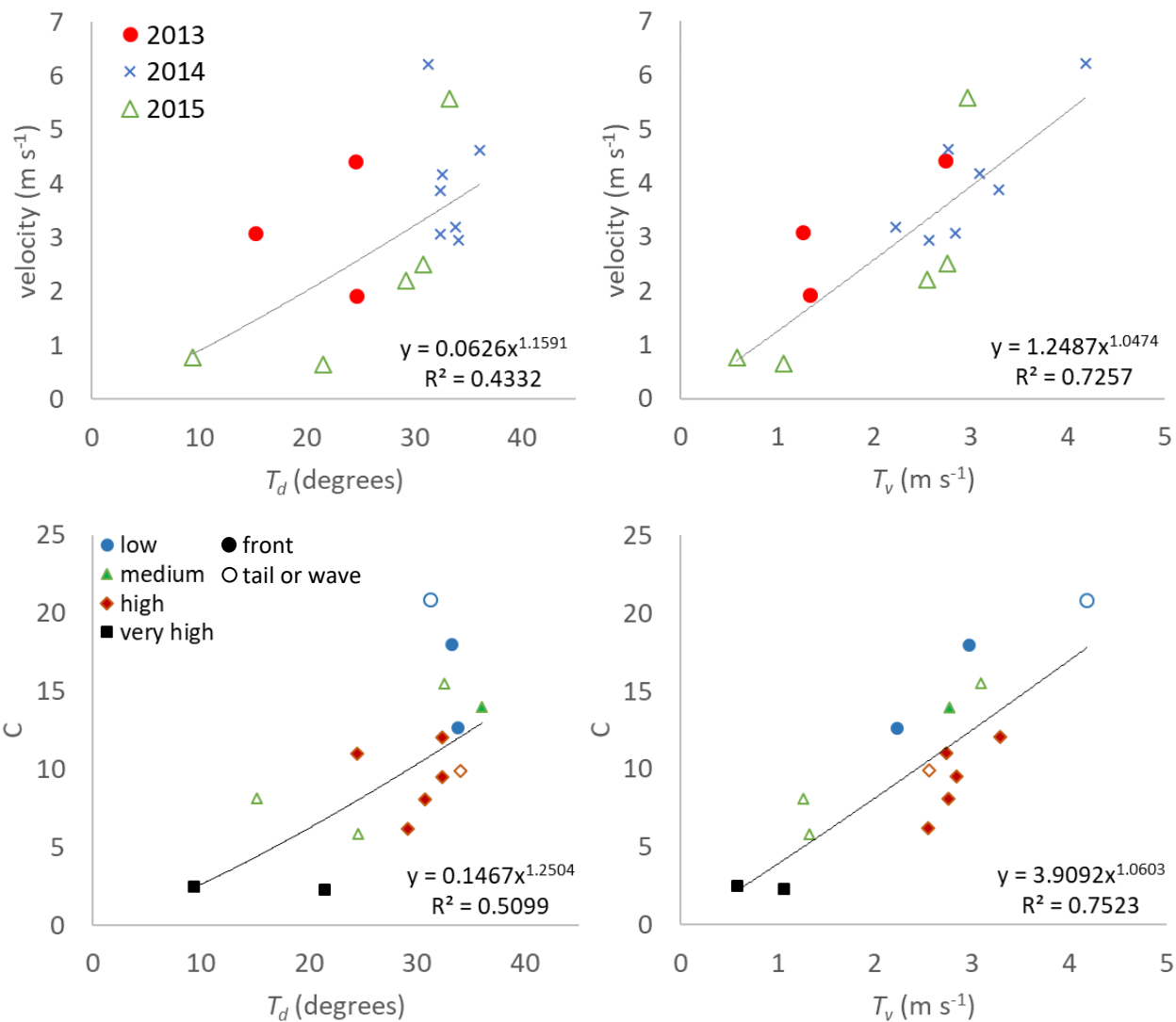


Figure 9: Classified by events (top), the directional turbulence index (T_d) (left) and velocity turbulence index (T_v) (right) are compared to LSPIV average surge velocity (top). Classified by visually estimated sediment concentrations (bottom) from Table 2, the T_d and T_v are compared to the flow resistance coefficient (C) (Eq. 1).

6 Conclusions

We have presented LSPIV-derived velocities for three debris flow events in the Gadoria channel, for a total of 11 surges and these velocities were compared with manual measurements on the ortho-rectified imagery (mean difference of -0.1 m s^{-1}) and upstream radar sensors (mean difference of -0.9 m s^{-1}). LSPIV appears to be a reliable method for measuring velocities of such flows, and to the best of our knowledge, this is one of the first studies on the topic. The variation of vectors from the LSPIV was introduced as an index of horizontal turbulence according to directional variation (T_d) and velocity variation (T_v).

Within the studied reach, debris flows varied in velocity and turbulence among different events, among individual surges within an event, and even within each surge. Several contributing factors can explain the variation such as rainfall variability, activation of variable source areas, channel storage levels, check-dam failures, boulder and log jamming, and just the complex interactions between the channel dynamic and the flow. For example, the 2015 event distinctly had the largest variation of surge velocities and turbulence that most likely caused by the burst of rainfall distributed over most of the catchment, which in turn activated more source areas than other events. The 2013 debris flow showed that a gentle relief in the channel opening can influence the front material deposition but not decrease the mean front velocity because of the water surge passing through and around the unlocking boulders. A strong power-law relationship is found between velocity and the T_v as well as the flow resistance coefficient C in the empirical equation of Koch et al. (1998). We propose that the T_v measurement improves the flow resistance coefficient for estimating velocity and T_d gives a better representation of sediment concentration.

LSPIV application on debris flows has shown to be very effective but there still needs to be a better understanding of the spatial and time resolution and the influence of slope. Some suggestions can be made for this type of monitoring, such as 1) be sure that the minimum frame rate of the IP camera is high enough to capture the movement (≤ 2 fps, depending on the flow velocity) or use a fixed frame rate from an analog camera; 2) locate the cameras to a stable reach with high viewing positions that are perpendicular to the flow; and 3) overlap the study area directly over stage sensors for discharge measurements for proper analysis of turbulence. Further studies can also involve calibrating geophones with the turbulence measurements which are more easily distributed in the field.

Further research on LSPIV derived velocity and turbulence needs to address the influence of confinement and roughness of the channel bed. Debris-flow channels have intermediate and large-scale roughness that make flow velocities and turbulence more variable as flow heights decrease (Rickenmann and Recking, 2011; Ferguson, 2012). Large-scale roughness can effect the confinement of the channel such as a large boulder or a debris-flow levee. Pre-event high-resolution elevation models and their residual heights and standard deviations at varying scales (Cavalli and Marchi, 2008) will provide better insight on spatial distribution of debris-flow velocities when they are directly compared with LSPIV measurements.

344 **Acknowledgements**

345 Funding for this research came from the research project “Kinoflow” funded by the Autonomous Province of Bozen-
346 Bolzano. The debris-flow monitoring station of Gadria catchment is managed by the Civil Protection Agency of the
347 Autonomous Province of Bozen-Bolzano. A preliminary analysis of the debris-flow hydrograph conducted by V.
348 D’Agostino and F. Bettella (Department TeSAF, University of Padova) helped interpret the 2014 event. We also thank
349 Alexandre Hauet (EDF-DTG Grenoble) who provided guidance and advice for the Fudaa-LSPIV application.

350 **References**

351 Aigner J., Habersack H., Rindler R., Blamauer B., Wagner B., Schober B., Comiti F., Dell’Agnese A., Engel M., Liébault F.,
352 Bel C., Bellot H., Fontaine F., Piegay H., Benacchio V., Lemaire P., Ruiz-Villanueva V., Vaudor L., Cavalli M., Marchi L.,
353 Crema S., Brardinoni, F., Bezak N., Rusjan S., Mikoš M., Abel J., Becht M., Heckmann T., Rimböck A., Schwaller G.,
354 Höhne R., Cesca M., Vianello A., Krivograd Klemenčič A., Papež J., Lenzi M.A., Picco L., Moretto J., Ravazzolo D., Jäger
355 G. , Moser M., Hübl J., and Chiari M.: Sed ALP – Sediment Management in Alpine Basins (www.sedalp.eu), WP5 Report -
356 Sediment transport monitoring, 256 p., 2015.

357 Arattano, M. and Grattoni, P.: Using a fixed video camera to measure debris-flow surface velocity. Proceedings of the
358 Second International Conference on Debris-flow Hazards Mitigation: Mechanics, Prediction, and Assessment, Taipei, 16-18
359 August, 2000; Wieczorek, G., Naeser, N., Eds.; A.A. Balkema: Rotterdam, 2000; 273–281, 2000.

360 Arattano, M. and Marchi, L.: Video-derived velocity distribution along a debris flow surge, *Physics and Chemistry of the*
361 *Earth: Part B* 25 (8), 781-784, 2000.

362 Arattano, M., Marchi, L., and Cavalli, M.: Analysis of debris-flow recordings in an instrumented basin: confirmations and
363 new findings, *Natural Hazards and Earth System Science*, 12(3), 679-686, 2012.

364 Berti, M.R., Genevois, R., LaHusen, R.G., Simoni, A., and Tecca, P.R.: Debris flow monitoring in the Acquabona watershed
365 in the Dolomites (Italian Alps), *Phys. Chem. Earth, Part B*, 25(9), 707-715, 2000.

366 Cavalli M., and Marchi, L.: Characterisation of the surface morphology of an alpine alluvial fan using airborne LiDAR.
367 *Natural Hazards and Earth System Sciences*, 8 (2), 323-333, 2008.

368 Cavalli, M., Trevisani, S., Comiti, F., and Marchi, L.: Geomorphometric assessment of spatial sediment connectivity in small
369 Alpine catchments, *Geomorphology*, 188, 31-41, doi:10.1016/j.geomorph.2012.05.007, 2013.

370 Cavalli, M., Goldin, B., Comiti, F., Brardinoni, F., and Marchi, L.: Assessment of erosion and deposition in steep mountain
371 basins by differencing sequential digital terrain models, *Geomorphology*, 291, 4-16, doi:10.1016/j.geomorph.2016.04.009,
372 2017.

373 Chen, C.L.: Comprehensive review of debris flow modeling concepts in Japan, In: J.E. Costa, G.F. Wieczorek (Eds.),
374 *Reviews in engineering geology*, vol VII. Debris flows/ avalanches: process, recognition, and mitigation., Boulder, CO, 13-
375 29, 1987.

376 Coe J.A., Kinner D.A., Godt J.W.: Initiation conditions for debris flows generated by runoff at Chalk Cliffs, central
377 Colorado, *Geomorphology*, 96, 270–297, 2008.

378 Comiti F., Marchi L., Macconi P., Arattano M., Bertoldi G., Borga M., Brardinoni F., Cavalli M., D’Agostino V., Penna D.,
379 and Theule J.: A new monitoring station for debris flows in the European Alps: first observations in the Gadria basin, *Nat*
380 *Hazards* 73:1175–1198. doi:10.1007/s11069-014-1088-5, 2014.

381 Costa, J.E.: Physical geomorphology of debris flows. In: J.E. Costa, P.J. Fleisher (Eds.), *Developments and Applications in*
382 *Geomorphology*, Springer Verlag, 268–317, 1984.

383 D’Agostino, V. and Bertoldi, G.: On the assessment of the management priority of sediment source areas in a debris-flow
384 catchment, *Earth Surface Processes and Landforms*, 39 (5), 656–668, DOI: 10.1002/esp.3518, 2014.

385 Ferguson, R. I.: River channel slope, flow resistance, and gravel entrainment thresholds, *Water Resources Research* 48:
386 W05517. DOI: 10.1029/2011WR010850, 2012.

387 Fujita, I., M. Muste, and A. Kruger: Large-scale particle image velocimetry for flow analysis in hydraulic engineering
388 applications, *J. Hydraul. Res.*, 36(3), 397–414, 1998.

389 Genevois, A., Galgaro, R., and Tecca, P.R.: Image analysis for debris flow properties estimation, *Physics and Chemistry of*
390 *the Earth, Part C* 26, 623–631, 2001.

391 Hauet A., Creutin J.-D., and Belleudy P.: Sensitivity study of large-scale particle image velocimetry measurement of river
392 discharge using numerical simulation, *Journal of Hydrology* 349(1–2): 178–190, 2008.

393 Hungr, O., Evans, S.G., Bovis, M., and Hutchinson, J.N.: Review of classification of landslides of flow type, *Environmental*
394 *and Engineering Geoscience*, VII, 221–238, 2001.

395 Hungr, O., Morgan, G.C., and Kellerhals, R.: Quantitative analysis of debris torrent hazards for design of remedial measures,
396 *Canadian Geotechnical Journal*, 21, 663–677, 1984.

397 Hürlimann, M., Rickenmann, D., and Graf, C.: Field and monitoring data of debris-flow events in the Swiss Alps, *Canadian*
398 *Geotechnical Journal*, 40(1), 161–175, 2003.

399 Iverson, R.M.: The physics of debris flows. *Reviews of Geophysics*, 35(3), 245–296, 1997.

400 Jacquemart, M., Meier, L., Graf, C., and Morsdorf, M.: 3D dynamics of debris flows quantified at sub-second intervals from
401 laser profiles, *Nat Hazards* 89:785. doi.org/10.1007/s11069-017-2993-1.

402 Javernick L., Brasington J., and Caruso B.: Modelling the topography of shallow braided rivers using structure-from-motion
403 photogrammetry, *Geomorphology* 213: 166–182, 2014.

404 Koch, T.: Testing various constitutive equations for debris flow modelling. In: K.e.a. Kovar (Ed.), *Hydrology, Water*
405 *Resources and Ecology in Headwaters*, IAHS, Publ. No. 248, Merano, Italy, 249–257, 1998.

406 Le Boursicaud, R., Pénard, L., Hauet, A., Thollet, F., and Le Coz, J.: Gauging extreme floods on YouTube: application of
407 LSPIV to home movies for the post-event determination of stream discharges, *Hydrol. Process.* 30, 90–105, 2016.

408 Le Coz, J., Hauet A., Pierrefeu G., Dramais G., and Camenen B.: Performance of image-based velocimetry (LSPIV) applied
409 to flashflood discharge measurements in Mediterranean rivers, *J. Hydrol.*, 394(1), 42–52, 2010.

410 Le Coz J., Jodeau M., Hauet A., Marchand B., and Le Boursicaud R.: Image-based velocity and discharge measurements in
 411 field and laboratory river engineering studies using the free Fudaa-LSPIV software, Proceedings of the International
 412 Conference on Fluvial Hydraulics, RIVER FLOW 2014, 1961–1967, 2014.

413 Marchi, L., Arattano, M., and Deganutti, A.M.: Ten years of debris-flow monitoring in the Moscardo Torrent (Italian Alps),
 414 Geomorphology, 46, 1-17, 2002.

415 McCoy, S.W., Kean, J.W., Coe, J.A., Staley, D.M., Wasklewicz, T.A., and Tucker, G.E.: Evolution of a natural debris flow:
 416 in situ measurements of flow dynamics, video imagery, and terrestrial laser scanning, Geology, 38(8), 735-738, 2010.

417 Muste, M., Hauet A., Fujita I., Legout C., and Ho H.-C.: Capabilities of large-scale particle image velocimetry to
 418 characterize shallow free-surface flows, Adv. Water Resour., 70(0), 160–171, doi:10.1016/j.advwatres.2014.04.004, 2014.

419 Navratil, O., Liébault, F., Bellot, H., Travaglini, E., Theule, J., Chambon, G., and Laigle, D.: High-frequency monitoring of
 420 debris-flow propagation along the Réal Torrent, Southern French Prealps, Geomorphology 201, 157–171, 2013.

421 Phillips, C.J. and Davies, T.R.H.: Determining rheological parameters of debris flow material, Geomorphology, 4, 101-110,
 422 1991.

423 Piermattei, L., Carturan, L., and Guarnieri, A.: Use of terrestrial photogrammetry based on structure-from-motion for mass
 424 balance estimation of a small glacier in the Italian alps, Earth Surf. Proc. Land., 40, 1791–1802, doi:10.1002/esp.3756, 2015.

425 Pierson, T.C.: Flow behavior of channelized debris flows, Mt. St. Helens, Washington, Hillslope Processes. Allen & Unwin,
 426 Boston, 1986.

427 Pierson, T.C. and Scott, K.M.: Downstream Dilution of a Lahar: Transition from Debris Flow to Hyperconcentrated
 428 Streamflow, Water Resources Research, 21(10), 1511-1524, 1985.

429 Prochaska, A.B., Santi, P.M., Higgins, J.D., and Cannon, S.H.: A study of methods to estimate debris flow velocity,
 430 Landslides, DOI 10.1007/s10346-008-0137-0, 2008.

431 Rickenmann, D.: Empirical relationships for debris flows, Natural Hazards, 19(1), 47-77, 1999.

432 Rickenmann, D. and Recking, A.: Evaluation of flow resistance in gravel-bed rivers through a large field data set, Water
 433 Resources Research 47: W07538. DOI: 10.1029/2010wr009793, 2011.

434 Rickenmann, D., Weber, D., and Stepanov, B.: Erosion by debris flows in field and laboratory experiments. In: D.
 435 Rickenmann, C.L. Chen (Eds.), Debris-Flow Hazards Mitigation: Mechanics, Prediction, and Assessment. Millpress,
 436 Rotterdam, The Netherlands, 883-894, 2003.

437 Scheidl, C., McArdeall, B.W., and Rickenmann, D.: Debris-flow velocities and superelevation in a curved laboratory channel,
 438 Can. Geotech. J. 52, 305–317, doi: 10.1139/cgj-2014-0081, 2014.

439 Stumpf, A., Augereau E., Delacourt C., and Bonnier J.: Photogrammetric discharge monitoring of small tropical mountain
 440 rivers: A case study at Rivière des Pluies, Réunion Island, Water Resour. Res., 52, doi:10.1002/2015WR018292, 2016.

441 Suwa, H., Okunishi, K., and Sakai, M.: Motion, debris size and scale of debris flows in a valley on Mount Yakedake, Japan,
 442 IAHS Publ. No. 217, 239–248, 1993.

443 Westoby, M. J., Brasington, J., Glasser, N. F., Hambrey, M. J., and Reynolds, J. M.: “Structure-from-Motion”
444 photogrammetry: A low-cost, effective tool for geoscience applications, *Geomorphology*, 179, 300–314,
445 doi:10.1016/j.geomorph.2012.08.021, 2012.

446